

Multimodality Inversion for Image Reconstruction of Objects Buried in Multilayered Media with Radar and Seismic Measurements

Qing H. Liu

Department of Electrical and Computer Engineering

Duke University

Durham, NC 27708

Email: qhliu@ee.duke.edu

www.ee.duke.edu/~qhliu

Joint Work with X. Millard, F. Li, L.-P. Song, and E. Simsek

Outline

- I. Introduction
- II. Theory of Forward and Inverse Solution in Layered Media
- III. 3D Single-Frequency EM Inversion
- IV. 2D Multi-Frequency EM and Seismic Inversion
- V. 2D EM/Seismic Joint Inversion in Layered Media
- VI. Summary and Future Work

I. Introduction

- Unique considerations for subsurface: Two important factors affecting subsurface EM imaging
 - Resolution and Depth of Penetration. These are two competing factors:
 - * Resolution improves with frequency
(but effects of clutters also become more severe)
 - * Penetration depth decreases with frequency because of attenuation
 - The frequency is dictated by the desired depth of interest. Thus we need to achieve the best resolution possible at the desired frequency

- Motivation
 - Electromagnetic and seismic measurements are complementary
 - Especially beneficial to combine these measurements for underground structures
 - Joint inversion can significantly improve inversion resolution
- Problem Considered
 - 2D and 3D EM/seismic scattering in multilayered media
 - Arbitrary number of layers are allowed
 - Such a model is necessary for the realistic situation where the soil and rock are heterogeneous

Problem Geometry

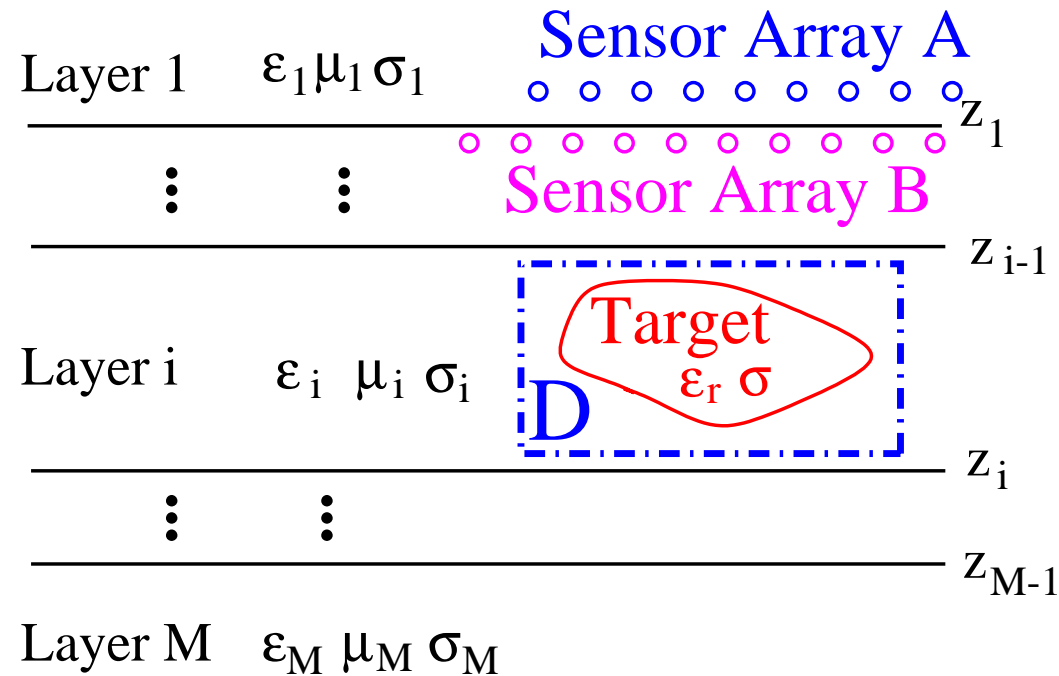


Figure 1: EM/Seismic measurements in a multilayered environment.

- Sources and receivers are located above, on, or under the surface.
- Parameters for seismic properties are not shown but are similar.
- The objective is to obtain a high-resolution image of the target.

II. Theory

- Electromagnetic Waves: The electric field satisfies

$$-\nabla \times \mu_r^{-1} \nabla \times \mathbf{E} + k_0^2 \epsilon_r \mathbf{E} = -j\omega \mu_0 \mathbf{J} \quad (1)$$

- Seismic Waves: The displacement vector satisfies

$$\frac{1}{2} \nabla \cdot [\mathbf{C} \cdot \{\nabla \mathbf{u} + (\nabla \mathbf{u})^T\}] + \omega^2 \rho \mathbf{u} = -\mathbf{f} \quad (2)$$

- Seismic Waves Become Scalar Acoustic Waves if Shear Waves are Neglected:
The pressure field satisfies

$$\rho \nabla \cdot (\rho^{-1} \nabla p) + k^2 p = -j\omega c^{-2} f_s \quad (3)$$

The Volume Integral Equation for 3D Heterogeneous Objects

- Assume the source is in layer p , receiver in layer m , and object in layer q .
- Fields in the m -th layer can be obtained once we have $\mathbf{D}_q(\mathbf{r})$ inside D :

$$\mathbf{E}_m^{scat}(\mathbf{r}) = -j\omega\left(1 + \frac{1}{k_m^2}\nabla\nabla\cdot\right)\mathbf{A}^{mq}(\mathbf{r}), \quad \mathbf{r} \in S$$

$$\mathbf{A}^{mq}(\mathbf{r}) = j\omega\mu_m \int_D \mathbf{G}^{mq}(\mathbf{r}, \mathbf{r}') \cdot \chi(\mathbf{r}')\mathbf{D}_q(\mathbf{r}')d\mathbf{r}'$$

where $\mathbf{G}^{mq}(\mathbf{r}, \mathbf{r}')$ is the **dyadic** Green's function for the magnetic vector potential in a multilayered medium; the contrast function is $\chi(\mathbf{r}) = [\epsilon(\mathbf{r}) - \epsilon_q]/\epsilon(\mathbf{r})$. The electric flux density $\mathbf{D}_q = \epsilon\mathbf{E}_q$.

- The volume EFIE within the object in the q -th layer is $\mathbf{E}_q^{inc} = \mathbf{E}_q - \mathbf{E}_q^{scat}$

$$\mathbf{E}_q^{inc}(\mathbf{r}) = \mathbf{E}_q(\mathbf{r}) + j\omega\left(\mathbf{I} + \frac{1}{k_q^2}\nabla\nabla\cdot\right)\mathbf{A}^{qq}(\mathbf{r}), \quad \mathbf{r} \in D$$

$$\mathbf{A}^{qq}(\mathbf{r}) = j\omega\mu_q \int_D \mathbf{G}^{qq}(\mathbf{r}, \mathbf{r}') \cdot \chi(\mathbf{r}')\mathbf{D}_q(\mathbf{r}')d\mathbf{r}'$$

The dyadic Green's function: No closed-form solution

$$G = \begin{bmatrix} G_{xx} & 0 & 0 \\ 0 & G_{xx} & 0 \\ G_{zx} & G_{zy} & G_{zz} \end{bmatrix}$$

Each component can be written as a Sommerfeld integral. For example, G_{xx}^{qq} component is

$$\begin{aligned} G_{xx}(\rho, z|z') &= \frac{1}{2\pi} \int_0^\infty \tilde{G}_{xx}(\mathbf{k}_\rho, z|z') J_0(k_\rho \rho) k_\rho dk_\rho \\ &= \frac{\mu_{rm}}{4\pi} \left\{ \int_0^\infty \frac{e^{-jk_{zq}|z-z'|}}{jk_{zq}} J_0(k_\rho \rho) k_\rho dk_\rho + \int_0^\infty \frac{k_\rho}{jk_{zq}} \frac{\sum_{i=1}^4 A_i}{A_5} J_0(k_\rho \rho) dk_\rho \right\} \\ &= \frac{\mu_{rm}}{4\pi} \left\{ \frac{e^{-jk_q r}}{r} + \int_0^\infty \frac{k_\rho}{jk_{zq}} \frac{\sum_{i=1}^4 A_i}{A_{TE}^p} J_0(k_\rho \rho) dk_\rho \right\} \end{aligned}$$

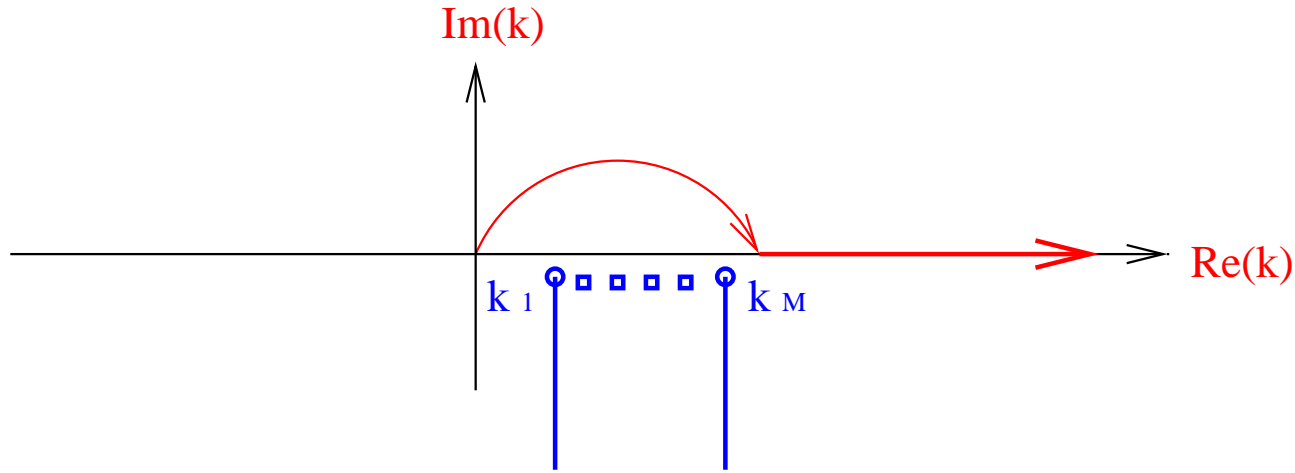


Figure 2: The Sommerfeld integration path)

For example, in 2D layered medium,

$$A_1 = \tilde{R}_{q,q-1} e^{-jk_{z,q}(-2z_q+(z+z'))}$$

$$A_2 = \tilde{R}_{q,q+1} e^{-jk_{z,q}(2z_{q+1}-(z+z'))}$$

$$A_3 = \tilde{R}_{q,q+1} \tilde{R}_{q,q-1} e^{-jk_{z,q}(2d_q-(z+z'))}$$

$$A_4 = \tilde{R}_{q,q+1} \tilde{R}_{q,q-1} e^{-jk_{z,q}(2d_q+(z+z'))}$$

$$A_5 = 1 - \tilde{R}_{q,q+1} \tilde{R}_{q,q-1} e^{-jk_{z,q}(2d_q)}$$

where $\tilde{R}_{i,j}$'s are generalized reflection coefficients between layers i and j .

Three tricks to significantly speed up the Sommerfeld integration:

- Primary field subtraction for sources and receivers in **all layers**
- Subtract the quasi-static field terms:

$$\lim_{k_\rho \rightarrow \infty} R_{i,i+1}^{TM} = \frac{\epsilon_{r,i+1} - \epsilon_{r,i}}{\epsilon_{r,i+1} + \epsilon_{r,i}} \quad (4)$$

$$\lim_{k_\rho \rightarrow \infty} R_{i,i+1}^{TE} = \frac{\mu_{r,i+1} - \mu_{r,i}}{\mu_{r,i+1} + \mu_{r,i}} \quad (5)$$

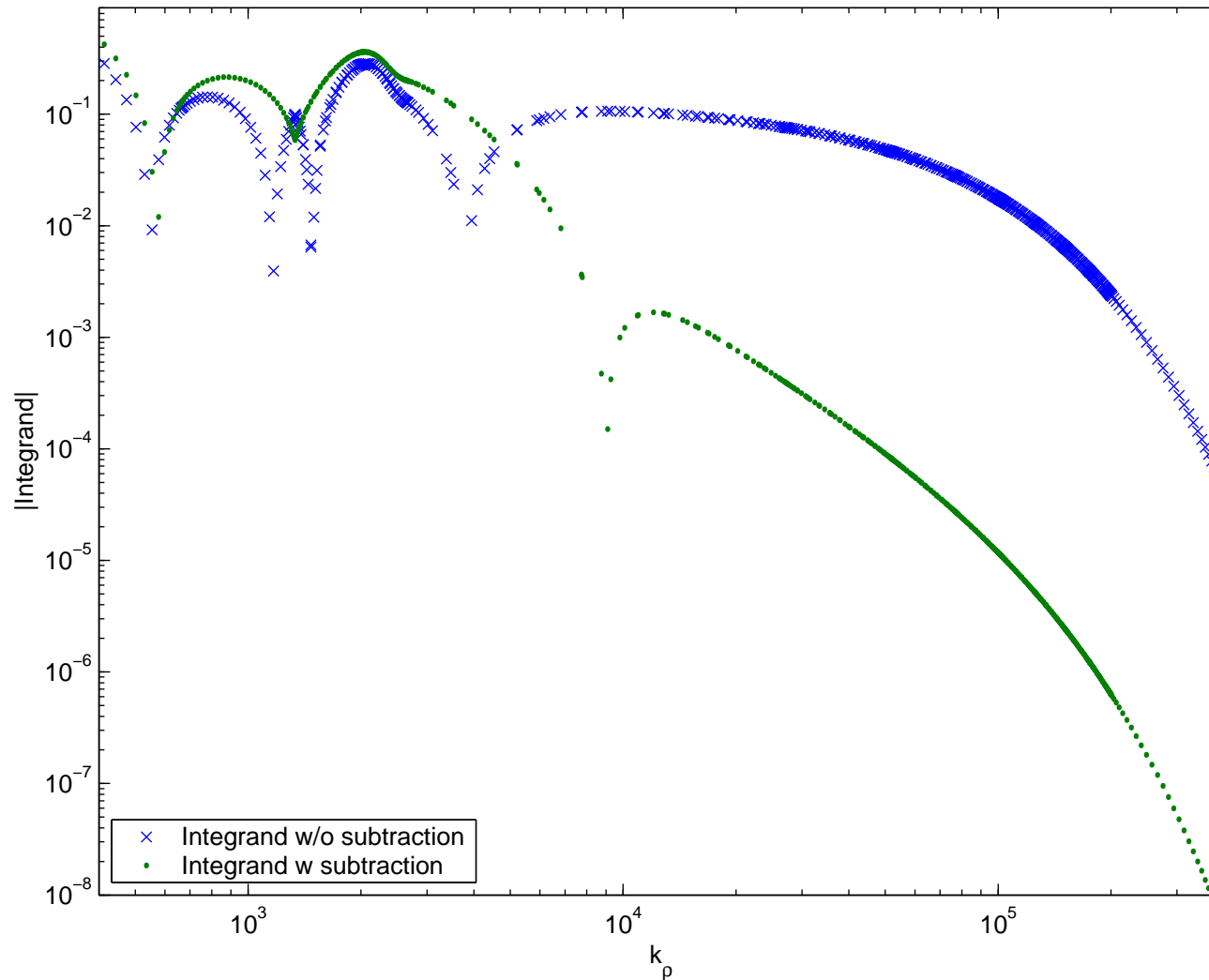
$$\lim_{k_\rho \rightarrow \infty} \tilde{R}_{i,i+1}^p = R_{i,i+1}^p \quad (6)$$

Closed-form solution for the quasi-static terms

$$\int_0^\infty e^{-k_\rho \gamma} J_1(k_\rho \rho) dk_\rho = 1 - \frac{\gamma}{\sqrt{\gamma^2 + \rho^2}} \quad (7)$$

- Adaptive numerical integration

Figure 3: The integrand with and without subtraction (2D case)



Similar for the 3D case.

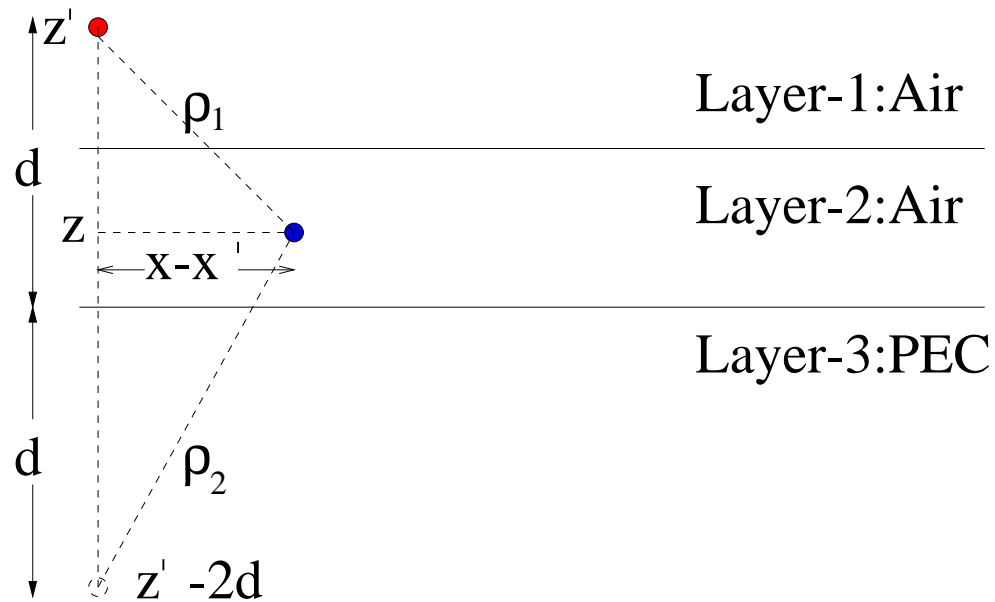


Figure 4: Two air layers above a PEC

$$f = 300 \text{ MHz}$$

$$\text{Exact Answer} = -\frac{j}{4} \left[H_0^{(2)}(k_0 \rho_1) - H_0^{(2)}(k_0 \rho_2) \right]$$

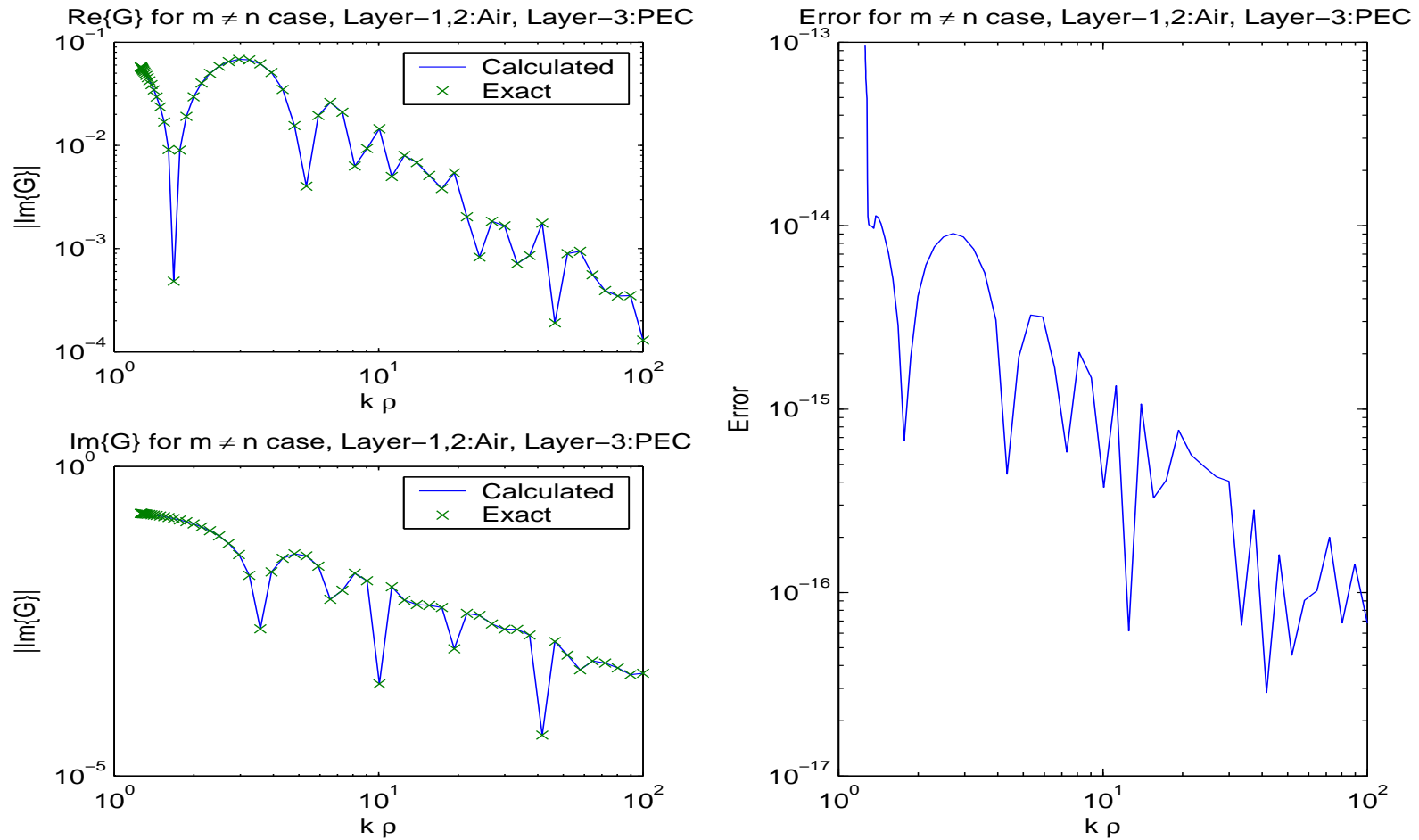


Figure 5: Real and imaginary parts of the Green's functions and magnitude of the relative error. **The accuracy is better than 10^{-13} .**

f=30 Ghz

<u>ϵ</u>	<u>z(mm)</u>
1.0	1.8
2.1	1.1
12.5	0.8
9.8	0.3
8.6	0.0
PEC	

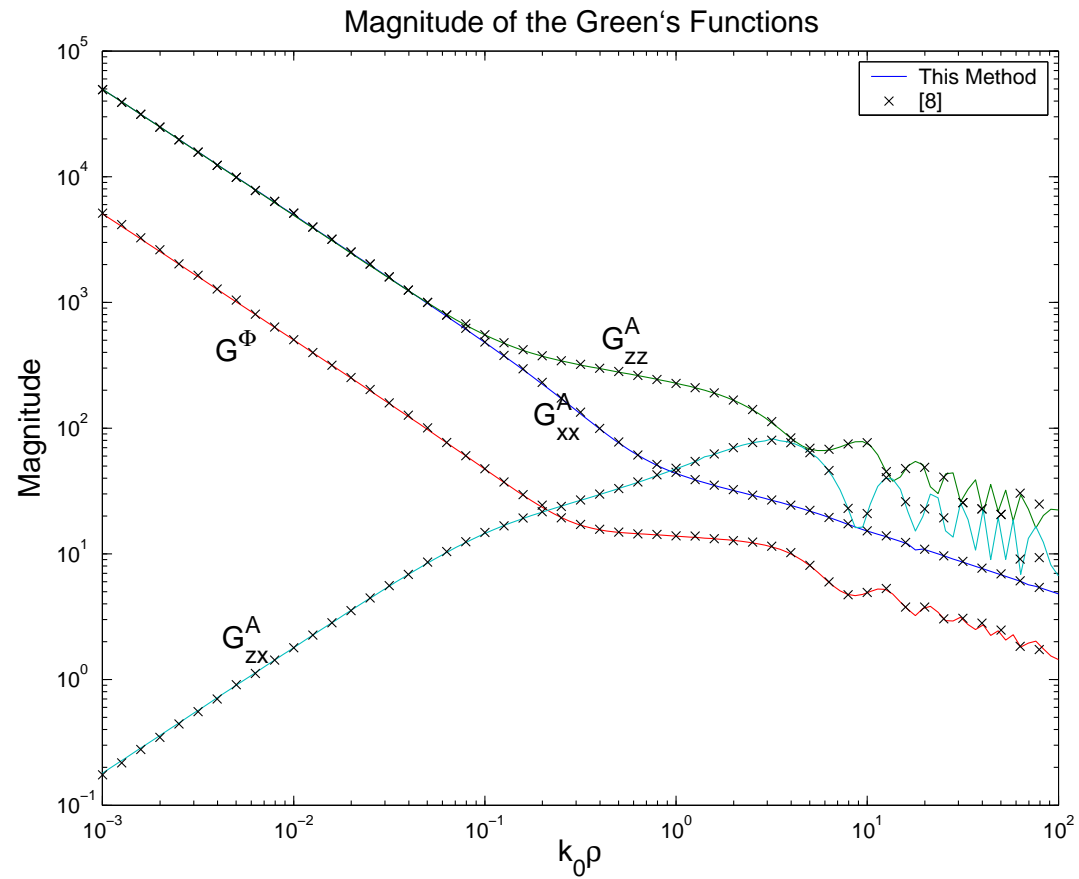


Figure 6: Magnitude of 3D Green's functions for a six-layer medium at 30 GHz. $z' = 0.4, z = 0.4$ mm.

The Fast Forward Method: The BCGS-FFT Method

- A stabilized biconjugate-gradient fast Fourier transform (BCGS-FFT) method has been developed for fast and accurate forward simulations of EM and acoustic waves in 3D and 2D multilayered media:

$$\mathcal{L}[\mathbf{D}_q(\mathbf{r})] = \mathbf{E}_q^{\text{inc}}(\mathbf{r}), \quad \mathbf{r} \in V \quad (8)$$

$$\mathcal{L}[\chi] = \frac{[\chi]}{\tilde{\epsilon}_q} - (k_q^2 + \nabla \nabla \cdot) \frac{1}{\tilde{\epsilon}_q} \int_V \mathbf{G}^{qq}(\mathbf{r}, \mathbf{r}') \cdot \chi[\mathbf{r}'] d\mathbf{r}'. \quad (9)$$

The BCGS-FFT method requires only $O(N \log N)$ CPU time and $O(N)$ memory.

Difficulty: The GF is no longer shift-invariant as in the free space.

Fortunately, the dyadic Green's function can be split into two terms:

$$\mathbf{G}^{qq}(\mathbf{r}, \mathbf{r}') = \mathbf{G}_-^{qq}(x - x', y - y', z - z') + \mathbf{G}_+^{qq}(x - x', y - y', z + z')$$

Thus, the FFT can be used to accelerate the Green's operations. **Refs:**

[1] Xu and Liu, *IEEE Antennas Wireless Propagat. Lett.*, 2002.

[2] Millard and Liu, *IEEE Trans. Antennas Propagat.*, 2003.

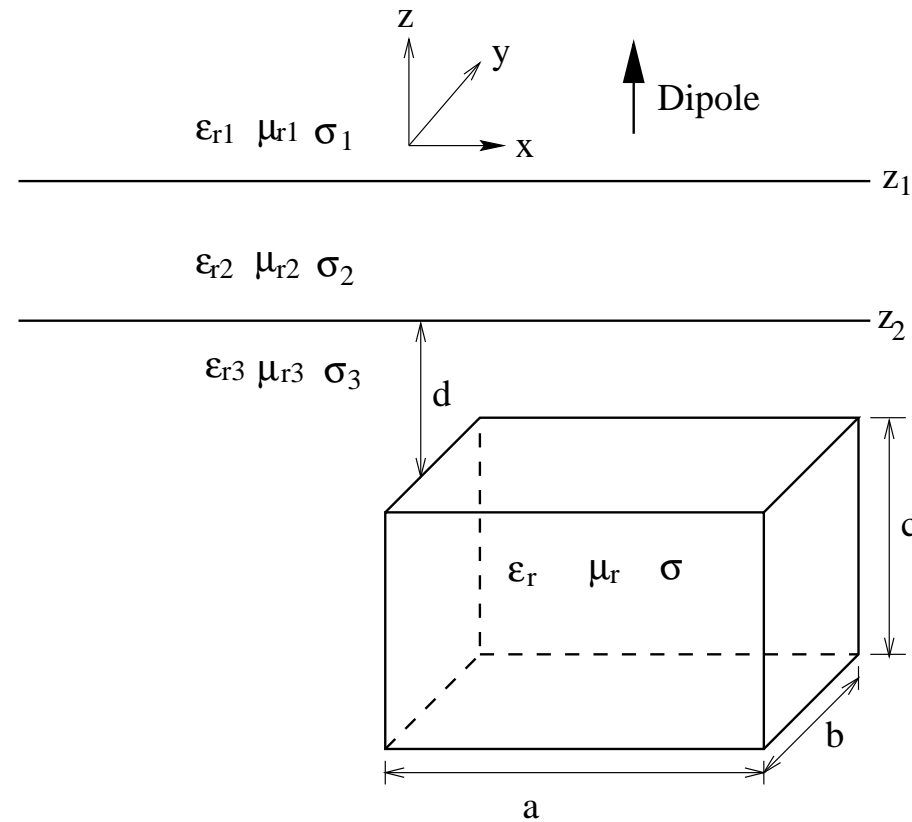


Figure 7: A 3-layer example with $(\epsilon_r, \sigma) = (1, 0)$, $(1.21, 0)$, $(1.44, 0)$, and $(9, 0.02)$ for the 3 layers and the object, respectively; $z_1 = 3.25$ and $z_2 = 2.75$ m, $d = 0.35$ m, $a = b = 1.6$ m and $c = 1.15$ m. The object center is at $(2.05, 2.05, 1.825)$ m, and the vertical electrical dipole is located at $\mathbf{r}_0 = (2.1, 2.1, 3.675)$ m.

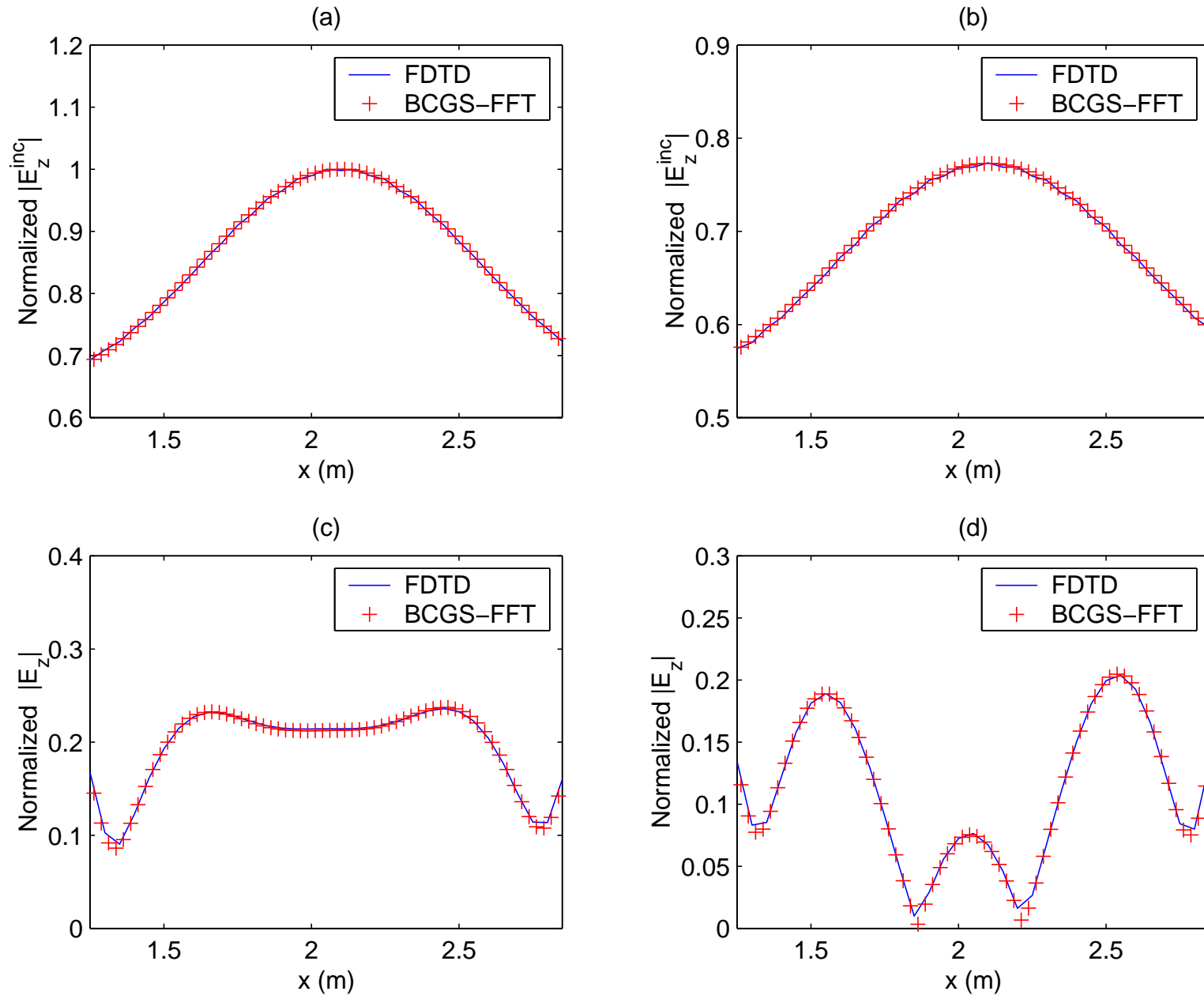


Figure 8: (a) Normalized incident field E_z^{inc} at $y = 1.9$ m, $z = 2.125$ m. (b) Normalized incident field E_z^{inc} at $y = 2.1$ m, $z = 1.875$ m. (c) Normalized total

Computational Complexity

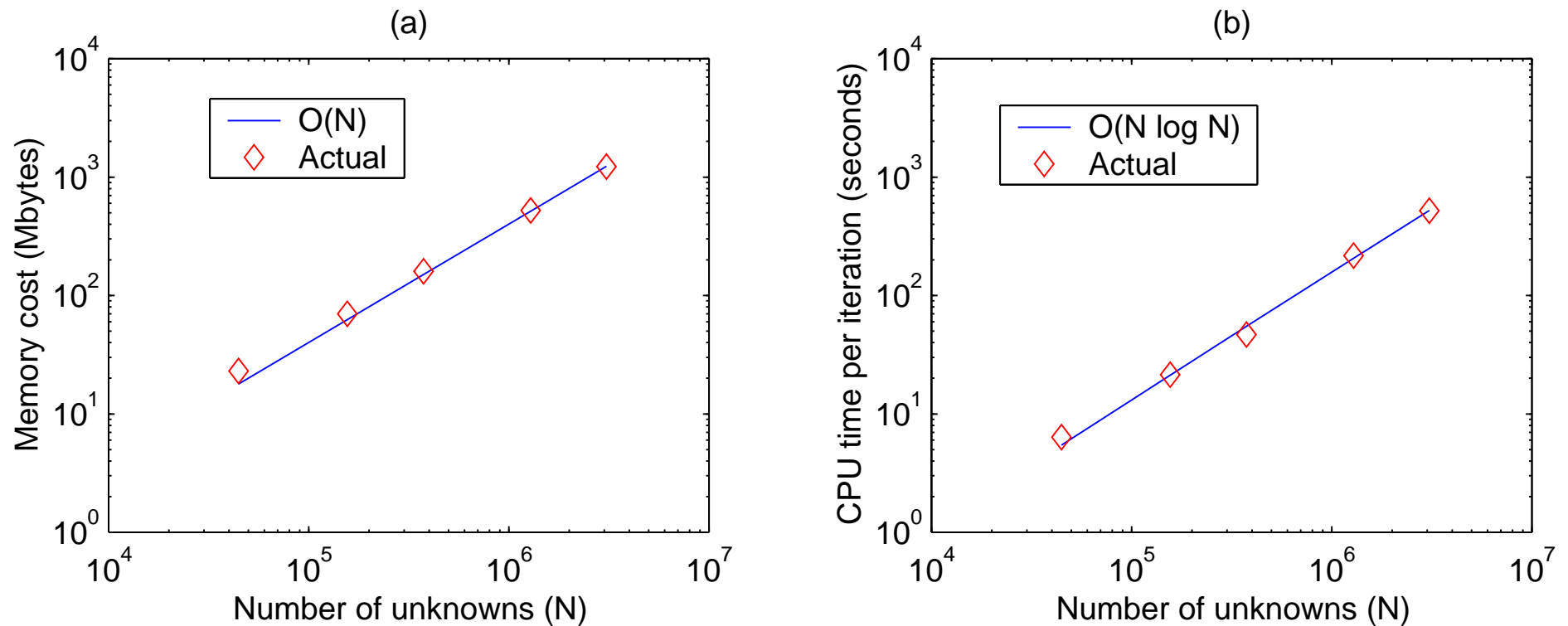


Figure 9: The computer memory is $O(N)$ (a), and CPU time is $O(N \log N)$ (b) versus the number of unknowns N .

The Nonlinear Inverse Scattering Methods

- Three methods have been developed:
 - The Born Iterative Method (BIM)
 - The Distorted Born Iterative Method (DBIM)
 - The Contrast Source Inversion (CSI) Method
- Summary of DBIM for the Inversion of Contrast χ
 - $\delta\chi_{n+1} = \chi_{n+1} - \chi_n$ denotes the $(n + 1)$ -th iteration's update
 - D denotes an enclosing box around the target domain;
 S denotes the sensor surface.
 - \mathcal{G} denotes DBIM's nonlinear mapping from the contrast to the scattered field

$$\delta\mathbf{E}^{scat} = \mathcal{G}_D \delta\chi, \quad \mathbf{r} \in \mathbf{D}$$

$$\delta\mathbf{E}^{scat} = \mathcal{G}_S \delta\chi, \quad \mathbf{r} \in \mathbf{S}$$

- Distorted Born Iterative Method

$$F = \|\delta f_{n+1} - \mathcal{G}_n \delta \chi_{n+1}\|^2 + \gamma \|\delta \chi_{n+1}\|^2$$

- The conjugate-gradient method is used to minimize this functional. FFT is used to accelerate the iterations.
- DBIM is faster than BIM and CSI when the sources and receivers are collocated.

III. 3D EM Inversion

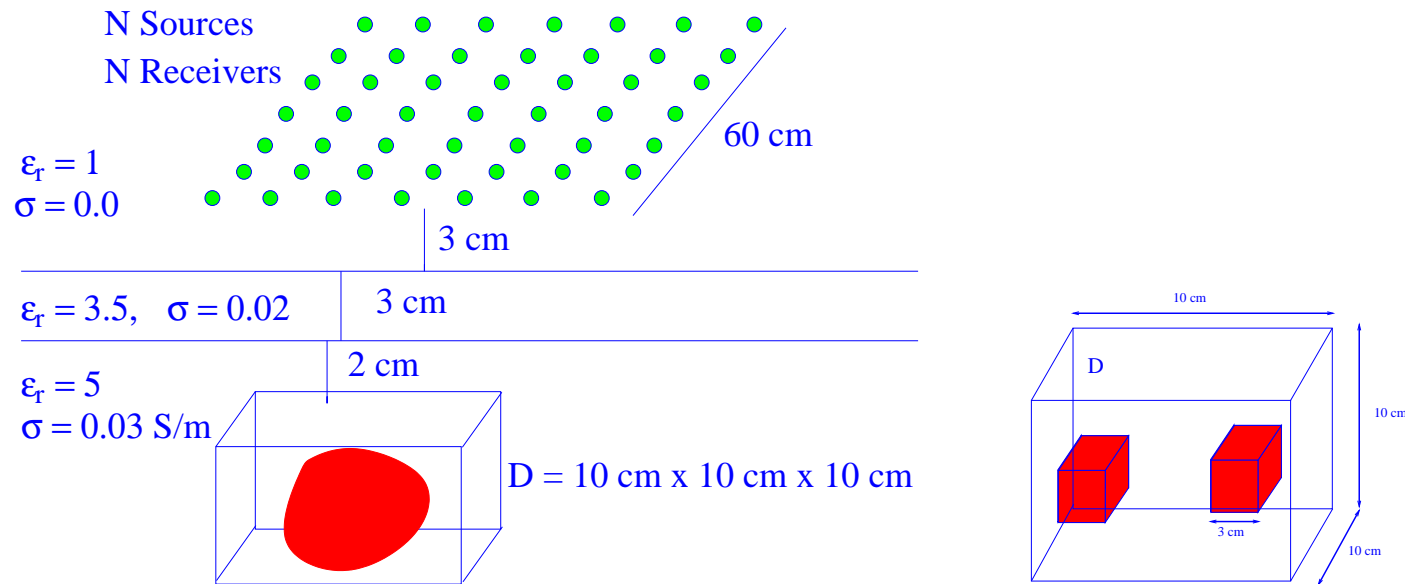


Figure 10: Typical configuration of an inhomogeneous object in a planarly layered medium. Right: Example of two targets ($\epsilon_r = 10, \sigma = 0.3 \text{ S/m}$).

- 64×64 sources/receivers in air. Single frequency at $f = 1 \text{ GHz}$.
- The 3-layer medium models the presence of top soil.

Noise Performance of 3D Inversion

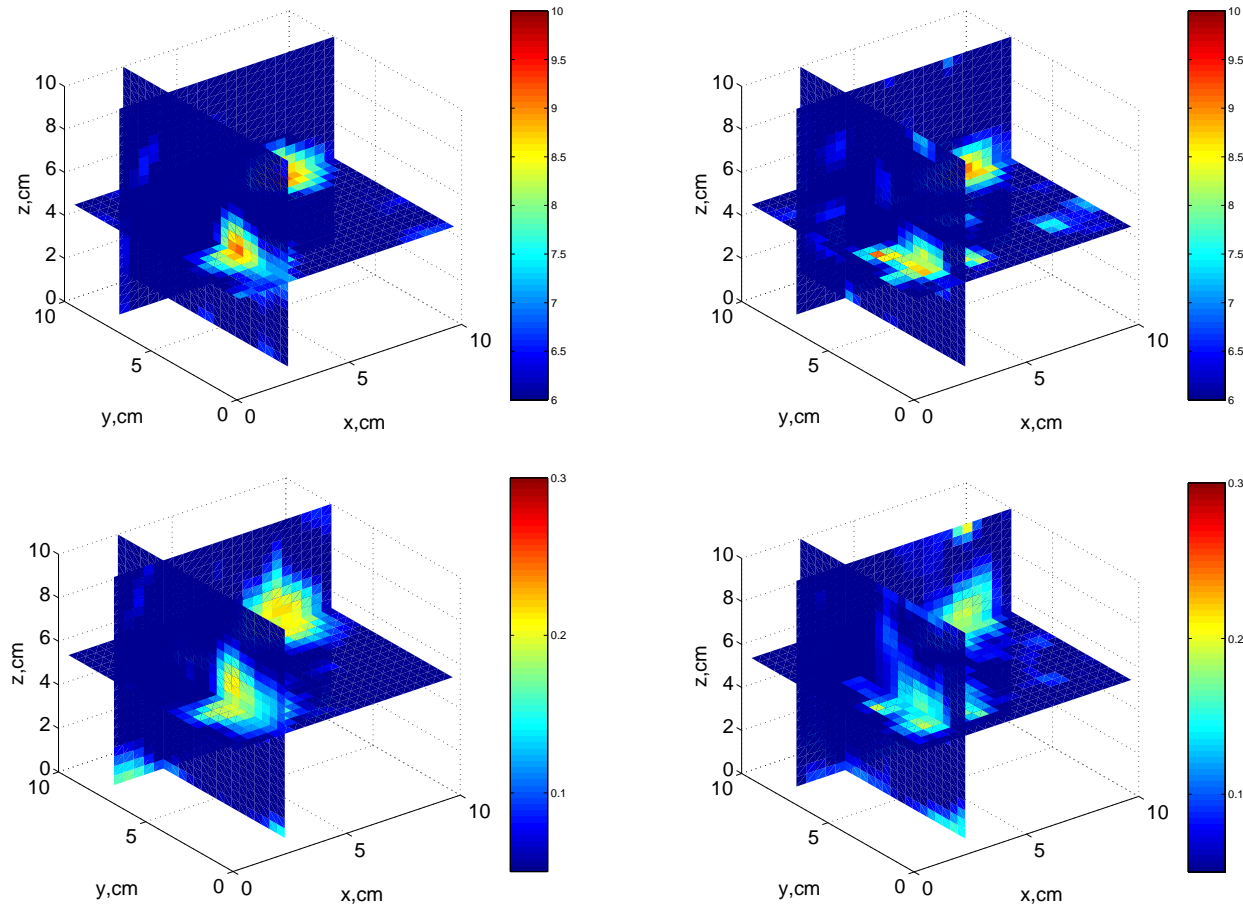
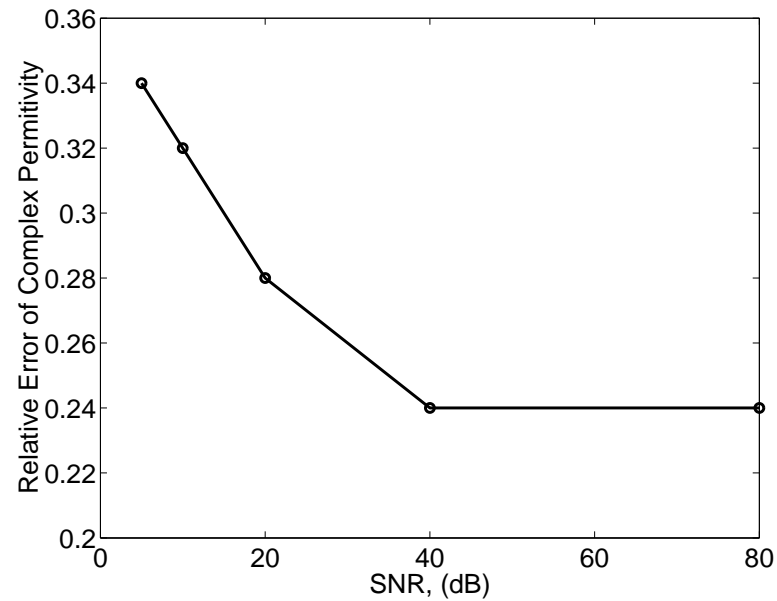


Figure 11: BIM (left) and DBIM (right) reconstruction for $\text{SNR} = 20$ dB. Top: dielectric constant ϵ_r . Bottom: conductivity σ .

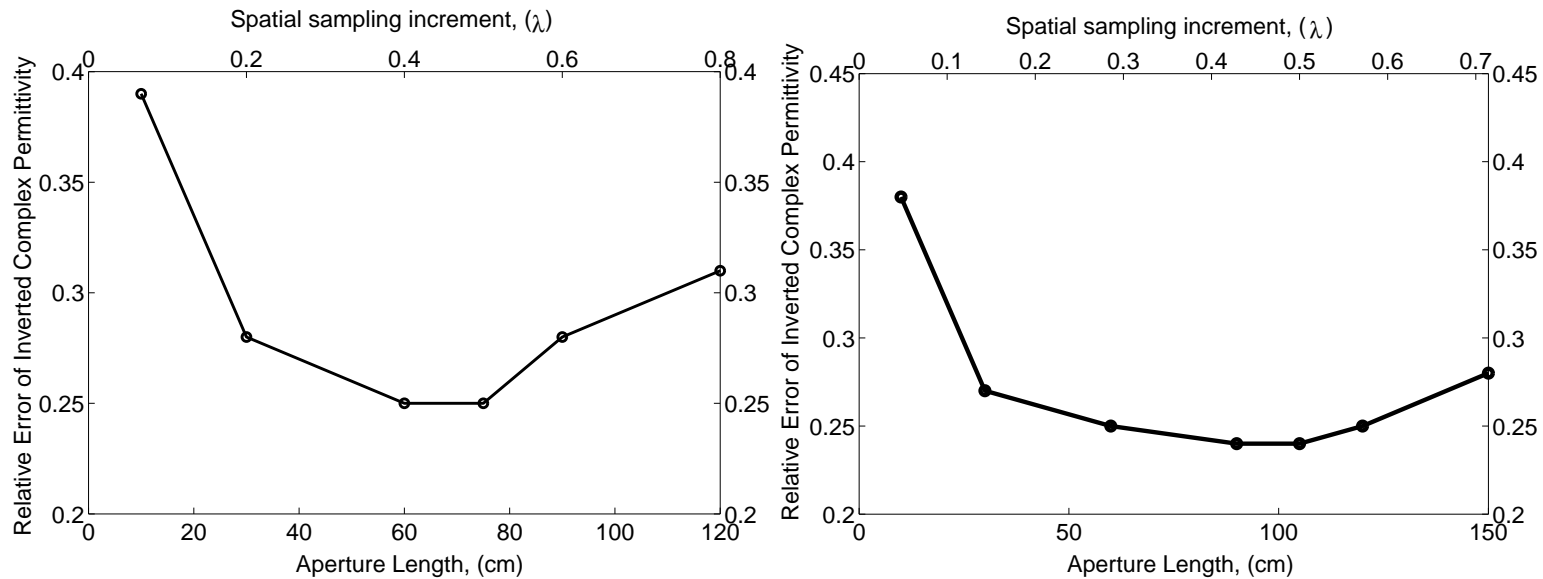
Relative Error of Complex Permittivity versus SNR

$$Err = \sqrt{\frac{\|\tilde{\epsilon}_t - \tilde{\epsilon}_i\|^2}{\|\tilde{\epsilon}_t\|^2}}$$



- The quality improves until SNR exceeds 40 dB

The Effect of the Aperture Size



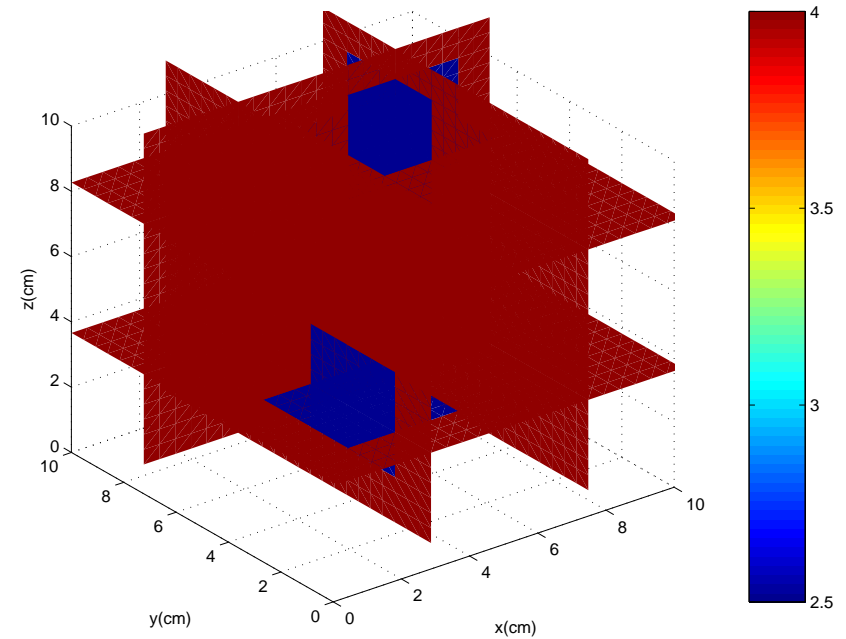
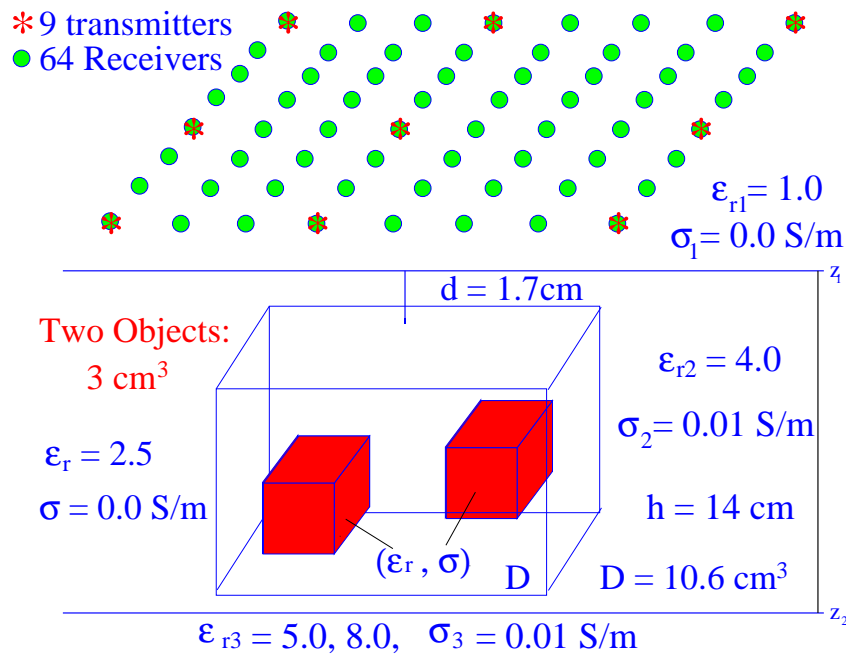
Relative error of inverted $\tilde{\epsilon}$ as a function of aperture size:

(a) Source/receiver numbers are 36/36

(b) Source/receiver numbers are 64/64.

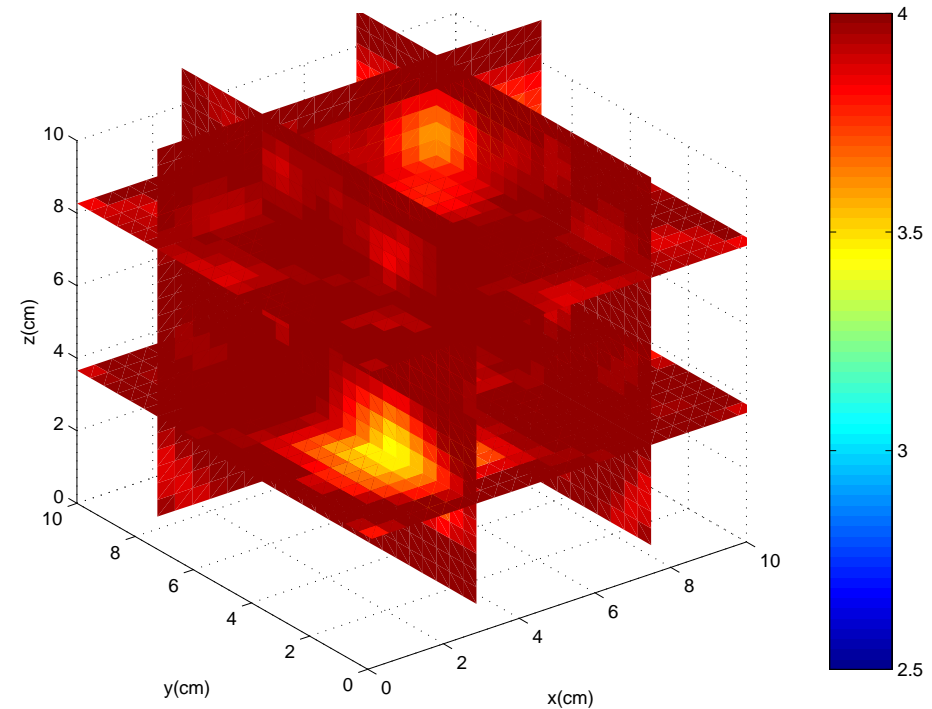
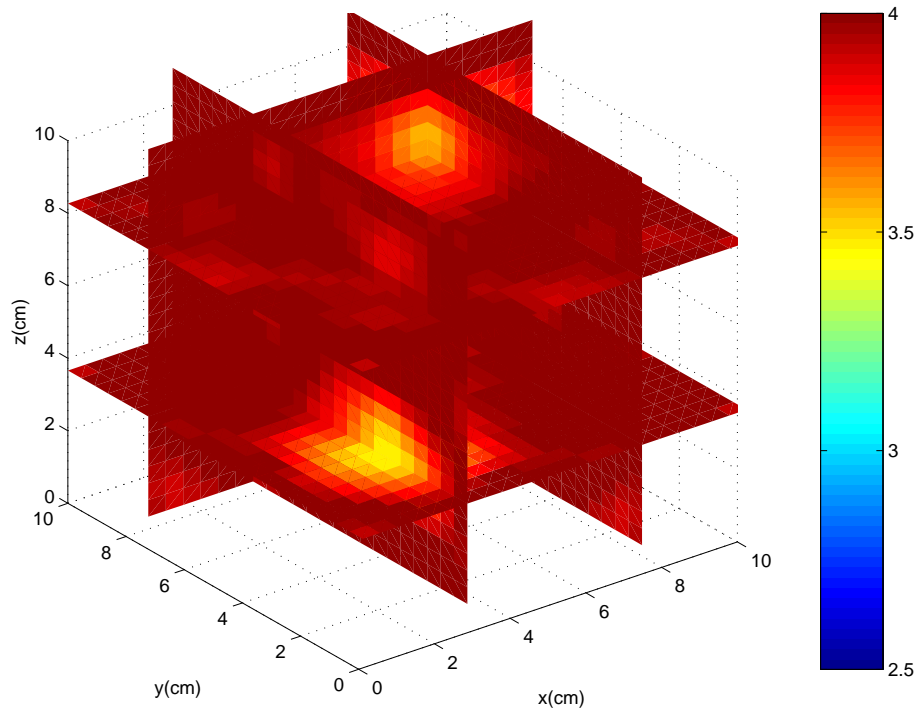
- The optimal sampling increment is about $\lambda_0/2$
- Further increase in aperture size beyond aperture-to-imaged-domain ratio of 6:1 (60 cm aperture) is not necessary.

Uncertainty in Layer 3: ϵ_{r3} is not exactly known for layer 3 A configuration and True Model



- Assuming that the third layer's parameters are not known exactly and using some estimated parameters of layer 2.

20% Uncertainty in Layer 3: $\epsilon_{r3} = 5.0$ is approximated by $\epsilon_{r3} = 4$

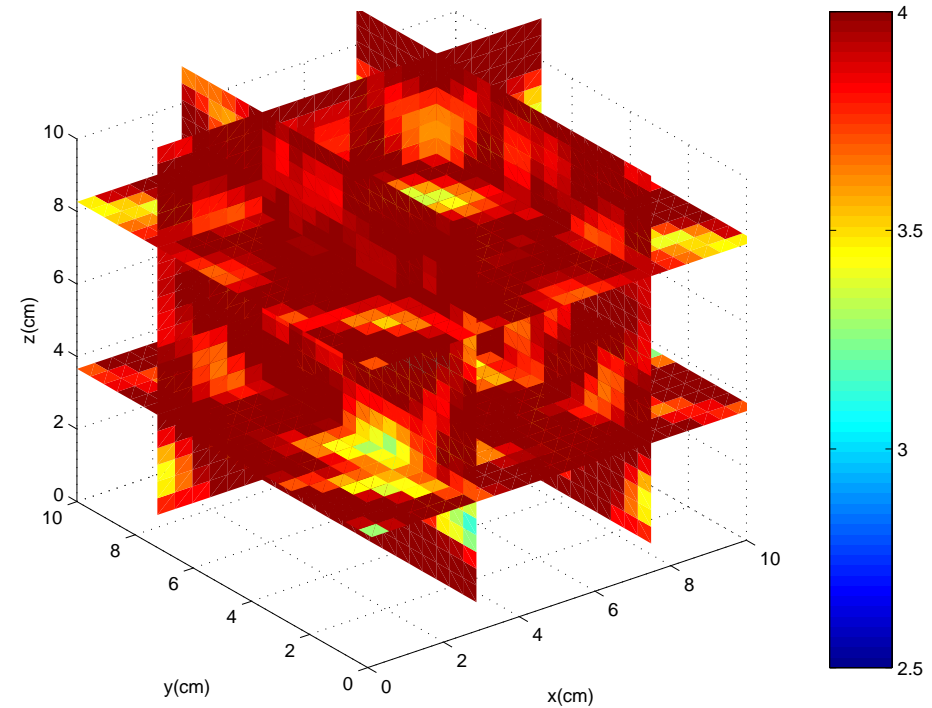
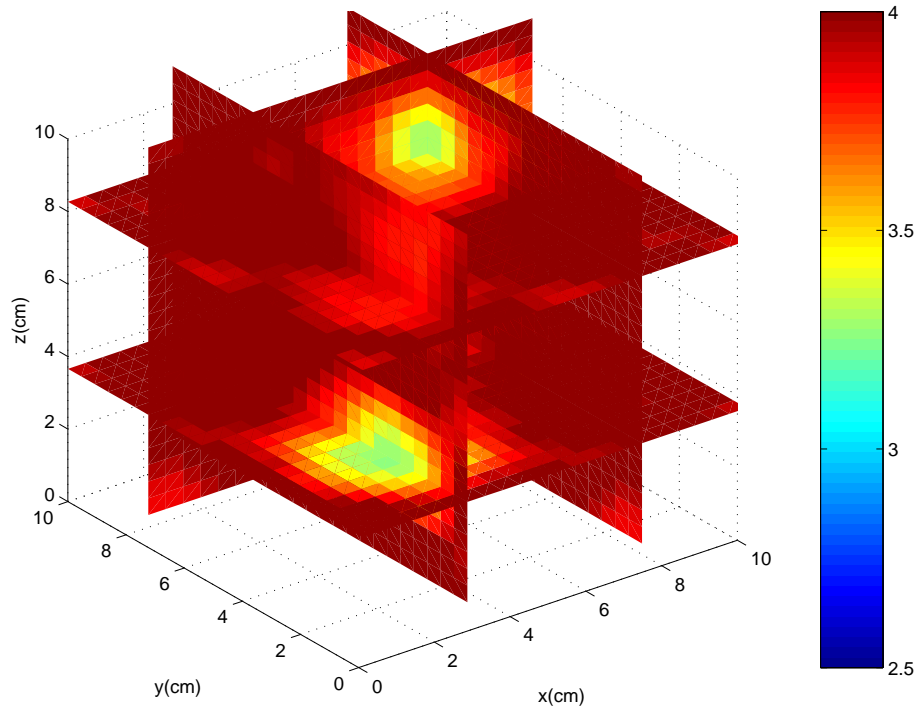


Left: Using exact information for layer 3: $\epsilon_{r3}=5.0$

Right: Using an approximate $\epsilon_{r3} = 4.0$ (20% error)

- The image is reasonably good with 20% uncertainty in layer 3

100% Uncertainty in Layer 3: $\epsilon_{r3} = 8.0$ is approximated by $\epsilon_{r3} = 4$



Left: Using a 3-layer background model with the correct $\epsilon_{r3}=8.0$

Right: Using a ϵ_r that is 100% smaller (i.e., $\epsilon_{r3} \approx 4.0$)

- Large contrast of layers 2 and 3 improves the image (mirror effect)
- Large uncertainty (100%) degrades the image

IV. 2D Multi-Frequency EM and Seismic Imaging

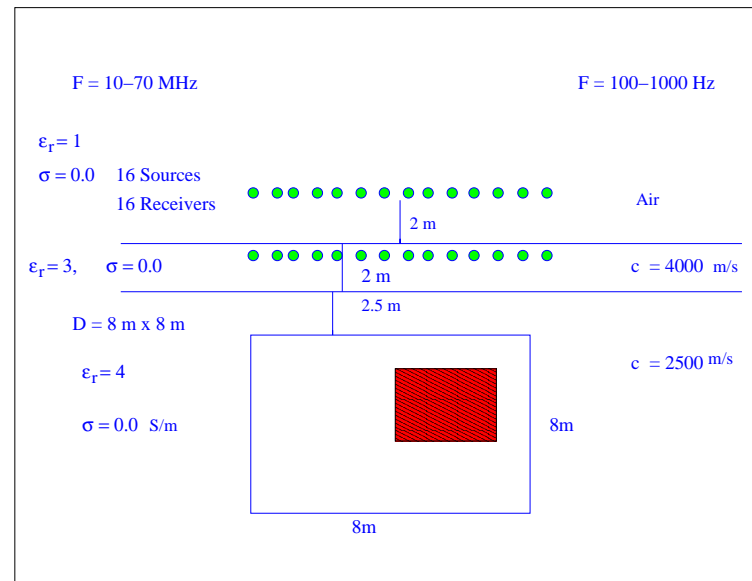


Figure 12: Configuration for seismic imaging of underground structures.

- 16×16 sources/receivers in the soil.
- The 3-layer medium models the presence of top soil.
- Shear Waves are neglected for such deep imaging cases for the seismic case.

DBIM for Multi-Frequency Inversion

For single-frequency inversion, we solve following equation:

$$\delta f_{n+1} = \mathcal{L}_n \delta \chi_{n+1}$$

For multi-frequency inversion, we solve following equations:

$$\delta f_{n+1, \omega_1} = \mathcal{L}_{n, \omega_1} \delta \chi_{n+1}$$

$$\delta f_{n+1, \omega_2} = \mathcal{L}_{n, \omega_2} \delta \chi_{n+1}$$

...

$$\delta f_{n+1, \omega_K} = \mathcal{L}_{n, \omega_K} \delta \chi_{n+1}$$

The above equations can be further expressed as:

$$\delta F_{n+1} = \mathcal{L}_n \delta \chi_{n+1}$$

where $F_{n+1} = [f_{n+1, \omega_1}, f_{n+1, \omega_2}, \dots, f_{n+1, \omega_K}]^T$;

$\mathcal{L}_n = [\mathcal{L}_{n, \omega_1}, \mathcal{L}_{n, \omega_2}, \dots, \mathcal{L}_{n, \omega_K}]^T$

Single-Frequency Seismic Imaging of a Void

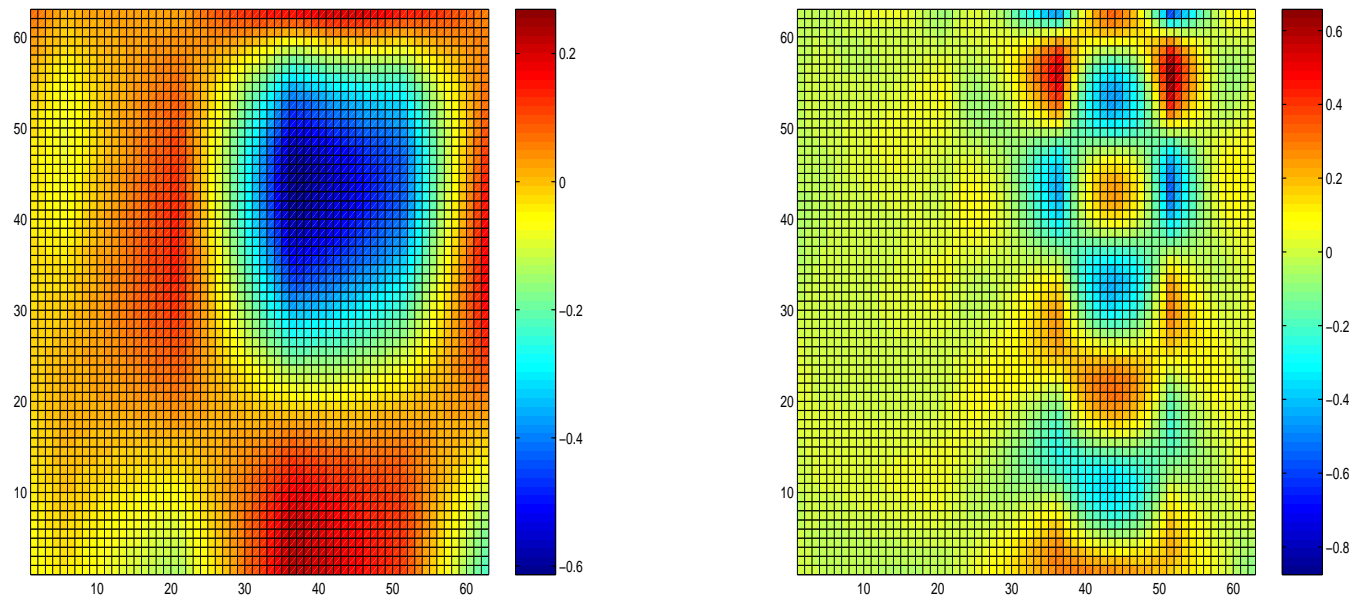


Figure 13: Left: 100 Hz. Right: 400 Hz

- The inversion at 100 Hz is reasonably good.
- At 400 Hz there are ghost images because of the inadequate sensors.

Multi-Frequency Seismic Imaging of a Void

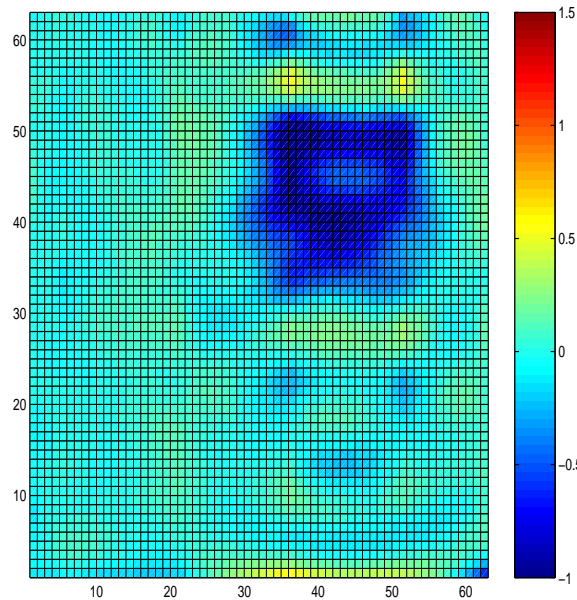


Figure 14: Imaging with 5 frequencies between 100–1000 Hz.

- Significant improvement is observed over the single-frequency imaging.

Multi-Frequency EM Imaging of an Underground Room

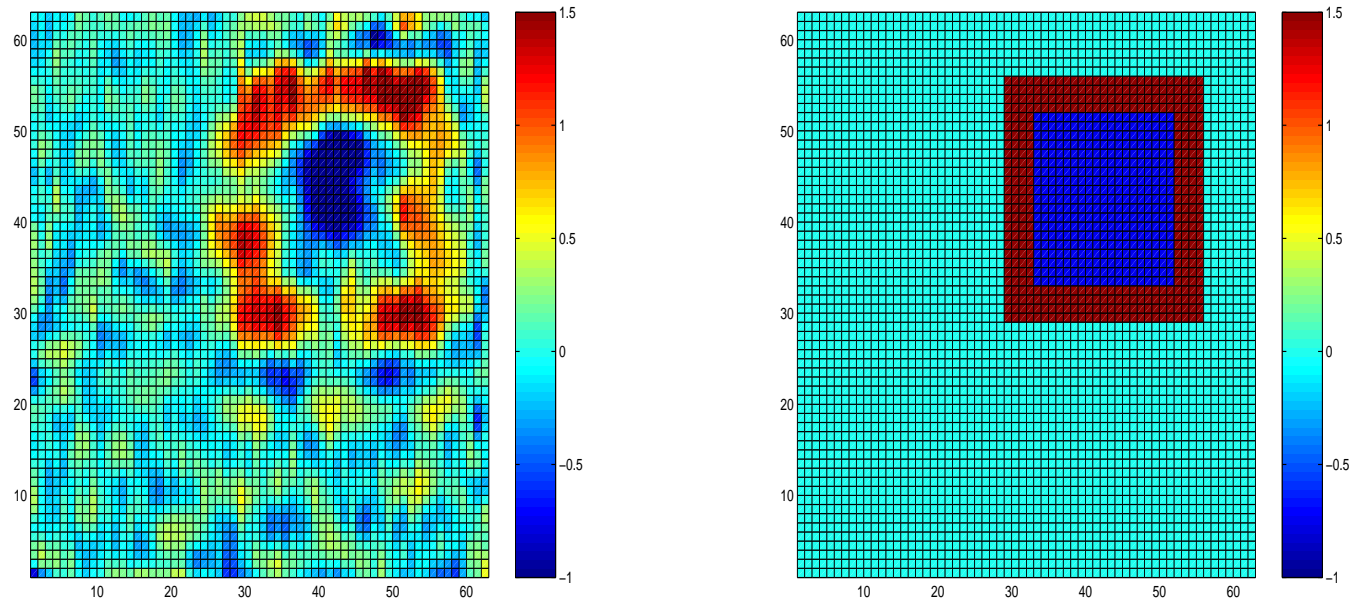


Figure 15: Imaging with 4 frequencies between 10–70 MHz.

Left: Reconstructed Image from multi-frequency EM data.

Right: The ground truth.

- The wall is well reconstructed because of its large EM contrast with background ($\chi = 1.5$).

Multi-Frequency Seismic Imaging of an Underground Room

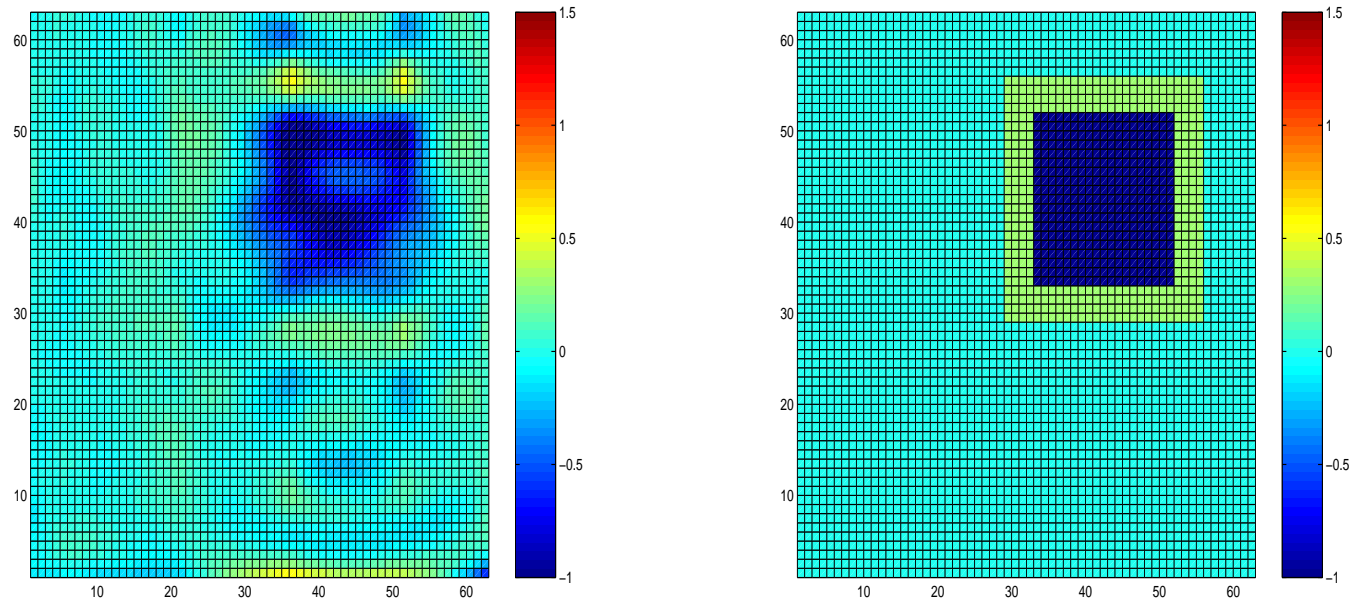


Figure 16: Imaging with 4 frequencies between 100–1000 KHz.

Left: Reconstructed Image from multi-frequency seismic data.

Right: The ground truth.

- The air inside is well reconstructed because of its large acoustic contrast with background.

Convergence Curves in Multi-Frequency Imaging

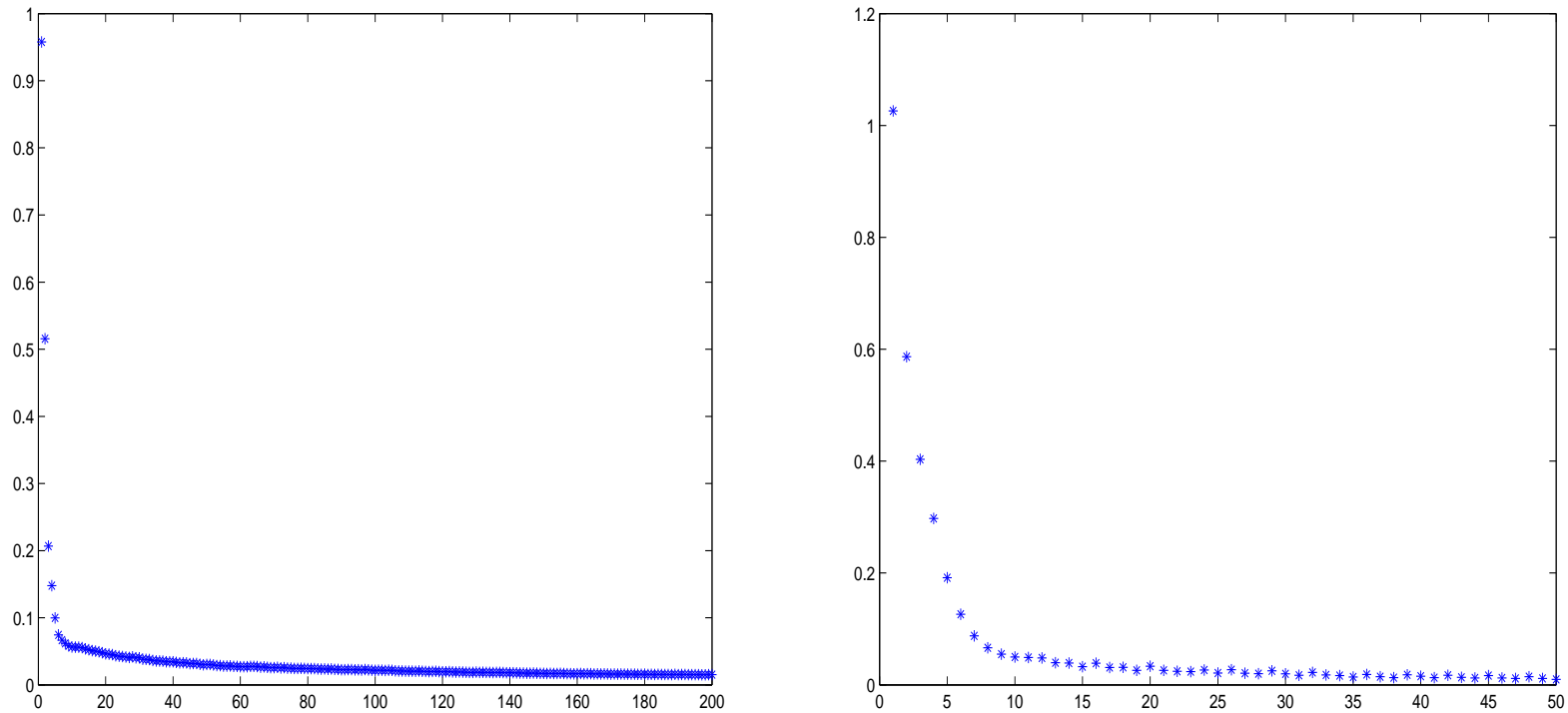


Figure 17: Data fitting error versus iteration number.

Left: EM inversion. Right: Seismic inversion.

V. 2D EM/Seismic Joint Inversion

- Joint Inversion using the Mutual Information (MI) Theory

MI of two random variables A and B can be obtained as:

$$I(A, B) = H(A) + H(B) - H(A, B)$$

where $H(A)$ and $H(B)$ are the entropies of A and B , and $H(A, B)$ is their joint entropy

$$H(A) = \sum -P_A(a) \log P_A(a)$$

$$H(B) = \sum -P_B(b) \log P_B(b)$$

$$H(A, B) = \sum -P_{A,B}(a, b) \log P_{A,B}(a, b)$$

The MI based criterion states that the images shall be registered when $I(A, B)$ is maximal.

The Mutual Information Theory

The probability density functions

$$P_{A,B}(a, b) = \frac{h(a, b)}{\sum h(a, b)}$$

$$P_A(a) = \sum_b P_{A,B}(a, b)$$

$$P_B(b) = \sum_a P_{A,B}(a, b)$$

P is the probability density function, $h(a, b)$ is the number of the corresponding pairs having intensity value a in the first image and intensity value b in the second image.

Mutual Information Theory in Joint EM/Seismic Inversion

Two modalities:

A–Seismic

B–EM

There exists an operator L_{BA} such that

$$L_{BA}B = A$$

The MI based criterion states that the images shall be registered when $I(A, L_{B,A}B)$ is maximal.

Mutual Information Theory in Joint EM/Acoustic Inversion

The output image is:

From the view of the “**Seismic Contrast**”, we have the combined image

$$\frac{A + L_{BA}B}{2}$$

From the view of the “**EM Contrast**”, we have the combined image

$$\frac{B + L_{AB}A}{2}$$

The consistency of L_{AB} and L_{BA} is measured by

$$\langle dp \rangle = \sum \|A - L_{BA}L_{AB}A\|$$

which is zero if the models are completely consistent. For simplicity we assume that

$$L_{BA} = L\mathbf{I}$$

in our preliminary study. This is an approximate model.

Joint EM/Seismic Inversion from the Seismic View

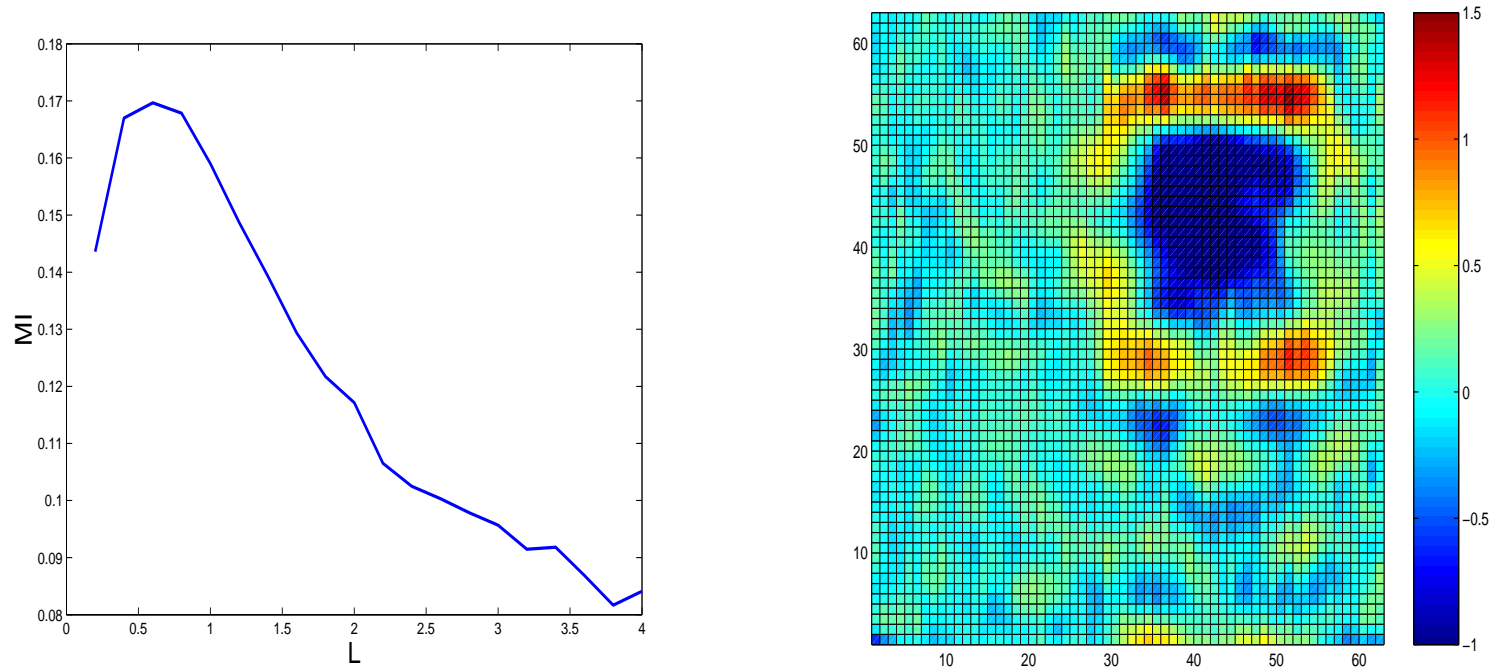


Figure 18: Joint inversion in the seismic view.

Left: The mutual information vs. L from the seismic view.

Right: The combined seismic image.

Joint EM/Seismic Inversion from the EM View

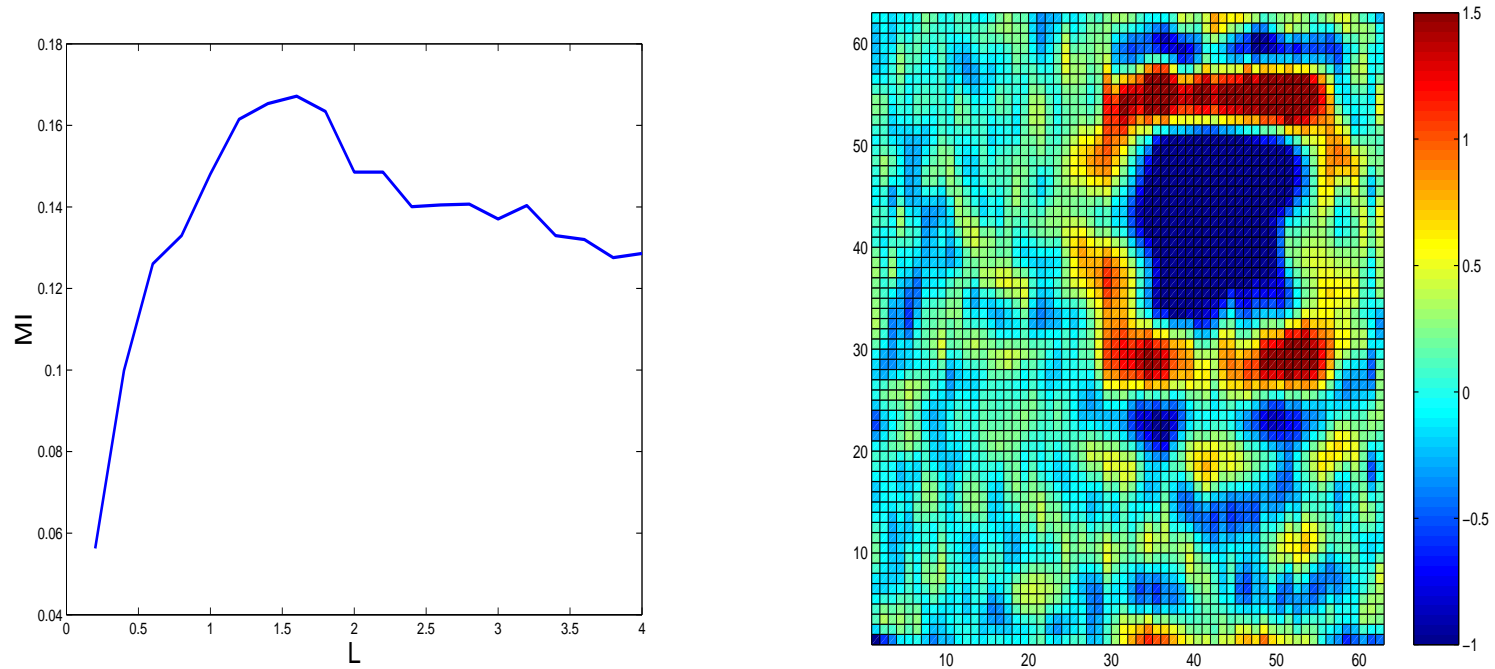
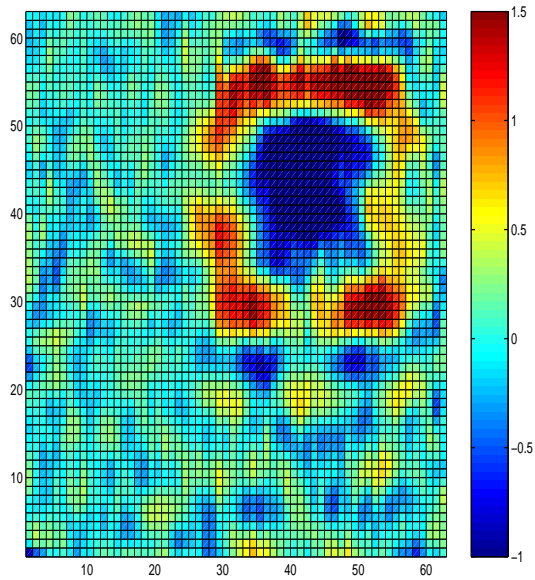


Figure 19: Joint inversion in the EM view.

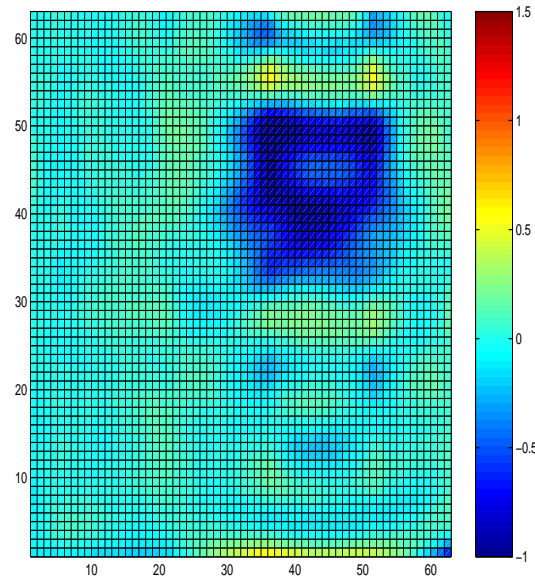
Left: The mutual information vs. L from the EM view.

Right: The combined EM image.

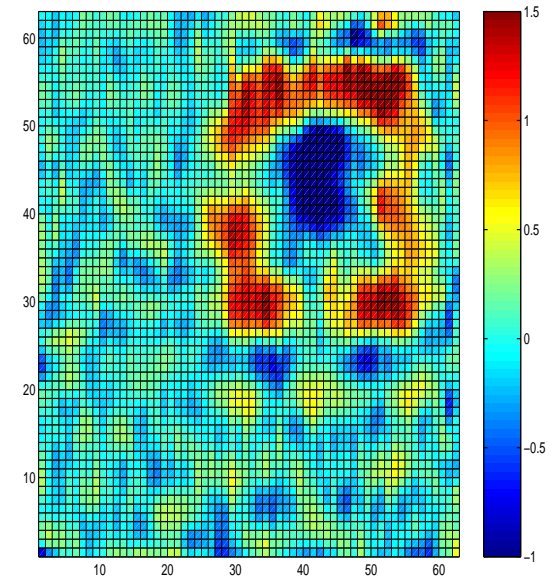
The Joint EM/Seismic Image versus Single-Modality Images



Joint Image $\alpha A + B$.



Seismic Image A .



EM Image B .

- The joint image is significantly better than single-modality images.

Summary and Future Work

- We have developed several new nonlinear inversion capabilities in layered media
 - 3D single-frequency EM inversion
 - 2D multi-frequency EM and seismic inversion
 - 2D EM/seismic joint inversion
- Multi-frequency inversion can significantly improve the resolution
- Joint inversion of multi-modalities has been demonstrated with synthetic EM and seismic data.
- Preliminary results are very encouraging in these new inversion models
- More thorough investigation is needed, especially in the area of combining multiple modalities. Inclusion of *a priori* correlation information.
- Work with measured data (W. Scott)